TRANSPORT OF ERODED SOIL PARTICLES

Bruce N. Wilson
H. Willard Downs
C. Tom Haan
and
Glenn A. Kranzler
Agricultural Engineering Department
Oklahoma State University

University Center for Water Research
Oklahoma State University
Stillwater, Oklahoma

October, 1988

ACKNOWLEDGEMENTS

The authors wish to acknowledge the creative efforts of Ms. Christine Rice and Mr. Mark Appleman in the design and implementation of equipment and software used in data collection. Their efforts were essential to the completion of the project. Experimental equipment was constructed and fabricated by the Agricultural Engineering Shop personnel under the supervision of Mr. Wayne Kiner. Their assistance is also greatly appreciated.

The research on which this report is based was financed in part by the United States Department of the Interior as authorized by the Water Research Development Act of 1979 (P.L. 95-467). Contents of this publication do not necessarily reflect the views and policies of the United States Department of the Interior. Mention of trade names is for informational purposes and does not necessarily imply endorsement.

INTRODUCTION

Statement of problem

Soil erosion and subsequent deposition are significant nonpoint pollution sources. They adversely affect the quality of our fluvial system by changing the aquatic life in streams and rivers, reducing the storage capacity of reservoirs and lakes, clogging navigable waterways, and transporting land-applied chemicals which otherwise would not enter the stream ecosystem. The movement of toxic chemicals in surface flows is often linked to the movement of eroded soil particles.

The most cost effective and environmentally safe method for solving sedimentation problems is to control erosion at its source, primarily upland erosion processes. An important component in upland erosion is the transport of eroded particles in rills. Usually the net delivery of soil to a waterway is less than that detached because of deposition in the upslope area. The net amount of soil to enter a stream's system is then determined by the transport rate. However, because of the tremendous variability in soil and runoff characteristics, it is difficult to extrapolate empirical transport rates obtained from one site to predict the response at a different site. An alternative to this approach is to model the transport rate theoretically.

Flows in rills and other erodible channels are frequently predicted by extending concepts developed for rigid or fixed boundary channels. Theoretically, flows in rigid channels can be solved using the equation of motion, the continuity equation and appropriate boundary conditions. As an example, consider uniform flow in a trapezoidal, concrete (fixed boundary) channel for a specified flow rate and known Manning's n and bed slope. Flow velocity and depth can be obtained by solving Manning's and continuity equations. A solution is possible because Manning's n, bed slope and channel cross sectional shape are considered independent of flow rate. This allows the effects of different flow parameters to be easily evaluated. For instance, the effects of changing bed slope can be predicted by simply using a different slope in Manning's equation.

Flows in erodible channels are considerably more complex than those in rigid channels. Erodible channels have the freedom to change their roughness, shape and bed slope with flow conditions. Hydraulic response is then dependent on sediment movement in the channel. These interactions make flow predictions more difficult. Consider, for example, the effects of changing bed slope on flow conditions in erodible channels. Such a change would affect the sediment response, which in turn, would alter hydraulic parameters such as Manning's n or cross sectional shape (e.g., trapezoidal to rectangular). If these parameters change significantly, additional relationships are needed to interrelate hydraulic and sediment responses.

Workers in fluvial hydraulics have proposed a number of empirical approaches to interrelate hydraulic and sediment responses (Leopold et al., 1964; Graf, 1971; Simons and Senturk, 1976). More intriguing, however, are those studies that have hypothesized an additional flow mechanism to supplement standard relationships of conservation of mass, force-momentum and/or energy. Many of these mechanisms are based on some minimization or maximization principle. Examples include various forms of minimum energy dissipation rate (Leopold and Langbein, 1962; Brebner and Wilson, 1967; Yang, 1971a; Chang and Hill, 1977 and others), minimum variance theory (Langbein and Leopold,1966), maximum sediment transport rate (White et al., 1982), and maximum friction factor (Davies and Sutherland, 1983). Based on the work of Song and Yang (1980) and Yang (1983), minimum energy dissipation rate appears to have the strongest theoretical base and to

explain a larger range of fluvial responses. This minimization principle is the focus of this study.

Objectives

The overall objective of this project is to gain a better understanding and to quantify the interactions between the hydraulic and sediment response in rills. To fullfill this objective, both theoretical and experimental work will be conducted. The specific objectives are given below:

1. To develop a predictive model for the erosion process in rills using minimum rate of energy concepts;

2. To gather data on the interactions between the flow rates, sediment loads, and rill geometry in a carefully controlled laboratory;

3. To conduct erosion runs in the field to quantify the geometry characteristics of these rills.

METHODOLOGY: THEORETICAL

DEFINITION OF ENERGY DISSIPATION RATE

Introduction

Minimum rate of energy dissipation has been proposed as an additional physical principle to describe flows in erodible channels. Originally this work was based on an analogy between fluvial and thermodynamic systems where an equivalent form of the Second Principle of Thermodynamics was developed for fluvial systems (Leopold and Langbein, 1962; Yang, 1971). This resulted in a hypothesis that a fluvial system will adjust itself to minimize the rate of potential energy dissipation per unit mass. Alternative formulations include minimum unit stream power (Yang, 1972), minimum total stream power (Chang and Hill, 1977) and minimum total stream power per unit length (Chang, 1979).

Important theoretical support for using minimum rate of energy dissipation in fluvial systems is given by Yang and Song (1979) and Song and Yang (1980). In these papers, minimum rate of energy dissipation is applied to open channel flows with rigid boundaries. They demonstrated that the equation of motion for steady, irrotational flows can be obtained by minimizing the rate of energy dissipation. Here energy dissipation rate is defined as the rate in which the mechanical energy of mean motion is lost either to viscous dissipation or to turbulent motion. Song and Yang (1979) showed that this approach can be used to predict velocity profiles for both laminar and turbulent flows. The true strength of this work, however, is that it provides theoretical support for using an analogy between open channel systems and thermodynamic systems. This basic definition, modified for two-phase flow, will be used in the proposed rill erosion algorithm.

Song and Yang (1980) assumed steady, irrotational, fixed boundary, single-phase fluid flow with zero velocity or zero shear along the channel boundaries in their theoretical development. The energy dissipation function in this paper will be written for two-phase flow of water and sediment. Unfortunately, rigorous development of this function is long. Only the key points will be given. A limited number of draft copies of the complete derivation (more than 100 typed pages) is available from the author.

Two-phase flow concepts

Sediment-laden flows are composed of water and sediment components. Each of these components can have different characteristics such as different velocities and densities. Emphasis in this study is on the properties of the bulk movement rather than those of its individual components as sometimes formulated (e.g., Standart, 1964; Whitaker, 1973; Gray, 1975).

It is desirable to treat the water-sediment mixture as a continuum so that continuous values can be assigned to each point in the flow field. Strictly speaking, the properties of the flow field are not continuous. Discontinuities exist at the interfaces between solid and liquid phases. This problem is handled by considering the point value as the average value over a given volume which encompasses enough particles to remove irregularities (Whitaker, 1969). If the length scale associated with the sediment particle is d, the length scale associated with the averaging or integration volume is ℓ, and the length scale associated with rill geometry (such as flow depth) is L, then a desirable characteristic of this averaging procedure is that $d \ll \ell \ll L$. If this characteristic is satisfied, areal-averaging of field variables is equal to volume-averaging (Whitaker, 1969). This is important in estimating surface forces and advection processes.

Field variables are volume-averaged using the general formulation given by Drew (1983) written for a generic variable F as

$$F = \frac{1}{V_t} \int_{V_t} \rho f \, dV \tag{1a}$$

where f is a local specific value, ρ is the local density and V_t is the volume. Because of the two-phase nature of the system, the product ρf will be defined as

$$\rho f = \rho_f f_f \delta_f + \rho_s f_s \delta_s \tag{1b}$$

where $\delta_f = 0$ when dV is in solid phase and $\delta_s = 0$ when dV is in liquid phase, otherwise these values are equal to one.

To illustrate the volume-averaging procedure, the results for two-phase density will be given. For volume-averaged density, f_s and f_f are equal to one. Therefore, Eq. 1a can be written as

$$\rho_m = \frac{1}{V_t} \left\{ \int_{V_s} \rho_s \, dV + \int_{V_f} \rho_f \, dV \right\} \tag{2a}$$

or

$$\rho_m = \rho_s \frac{V_s}{V_t} + \rho_f \frac{V_f}{V_t} \tag{2b}$$

where ρ_m, ρ_f and ρ_s are the densities of the mixture (bulk), fluid and solid phases, respectively, and V_f and V_s are the volume occupied by fluid and solid phases, respectively. Using volumetric concentration, mixture density can be written as

$$\rho_m = \rho_s c + \rho_f (1-c) \tag{3}$$

where c is the volumetric concentration of solids.

In a similar manner, a volume-averaged mixture velocity can be defined where f_s is equal to the velocity of the solid phase and f_f is equal to the velocity of the fluid phase. Mixture velocity can then be defined as

$$\rho_m u_{mi} = u_{si} \rho_s c + u_{fi} \rho_f (1-c) \tag{4}$$

where u_{mi}, u_{si} and u_{fi} are the mixture velocity, fluid velocity and solid velocity, respectively, in the ith direction.

Laminar flow equations

Using volume-averaging and areal-averaging techniques, fundamental relationships for conservation of mass, equation of motion, and energy equations have been derived for the bulk fluid. Non-linear spatial fluctuations around mean values were neglected. Additional terms were eliminated using an order of magnitude analysis.

The conservation of mass for two-phase, laminar flow can be written as

$$\frac{\partial \rho_m}{\partial t} + \frac{\partial \rho_m u_{mi}}{\partial x_i} = 0 \tag{5}$$

where tensor notation is used and ρ_m and u_{mi} are as previously defined. The mixture density is independent of time and space for constant volumetric concentration fluid.

The equation of motion for two-phase, laminar flow in the ith direction be written as

$$\frac{\partial \rho_m u_{mi}}{\partial t} + \frac{\partial \rho_m u_{mi} u_{mj}}{\partial x_j} = - \frac{\partial p}{\partial x_i} + \frac{\partial \tau^t_{ij}}{\partial x_j} + \rho_m g_i \tag{6}$$

where p is pressure, g_i is the gravitational component and τ^t_{ij} is the total shear stress defined as

$$\tau^t_{ij} = \tau^s_{ij}\, c + \tau^f_{ij}\, (1-c) \tag{7a}$$

where τ^f_{ij} and τ^s_{ij} are fluid-fluid and solid-solid shear, respectively. Much theoretical interest lies in estimating τ^t_{ij} (see Buyevich and Shchelchkova, 1978). A rough estimate of τ^t_{ij} will be obtained using the experimental results of Bagnold (1954, 1956). Total shear stress is evaluated as

$$\tau^t_{ij} = \mu_m \left\{ \frac{\partial u_{mj}}{\partial x_i} + \frac{\partial u_{mi}}{\partial x_j} \right\} \tag{7b}$$

where μ_m is a "mixture" viscosity defined using Bagnold's data as

$$\mu_m = g(\lambda)\mu_f \tag{7c}$$

where $g(\lambda)$ is a some function of linear concentration λ that could be estimated using Bagnold's experimental results and μ_f is the viscosity of water.

In laminar flow there are three energy equations of interest: (1) conservation of total energy (mechanical and heat energy), (2) mechanical energy equation, and (3) thermal energy equation. The conversion of mechanical energy to heat energy can be evaluated by examining these relationships, resulting in a energy dissipation rate term. Details of this

approach will only be given for turbulent flows.

Turbulent flow equations

Equations developed so far are for laminar flow conditions. Turbulent flows are usually considered by dividing instantaneous values into mean (now with respect to time) and fluctuating components. This procedure is similar to that used in volume-averaging, except the time frame is too large to neglect products of fluctuating components. To simplify mathematical manipulations, the concentration of solids is assumed independent of space and time. Mixture density and viscosity are then constants.

The conservation of mass for turbulent, two-phase flows is obtained by substituting mean and fluctuating components into Eq. 5 and time averaging the resulting expression. For constant mixture density, the conservation of mass for mean motion can be written as

$$\frac{\partial U_{mj}}{\partial x_j} = 0 \tag{8}$$

where U_{mj} is the mean velocity in the jth direction.

The equation of motion for mean flow is obtained by substituting mean and fluctuating components in Eq. 6 and again using time-averaging procedures. This procedure introduces an additional term because of the non-linear momentum flux rate. The equation of mean motion for turbulent flows can be written as

$$\frac{\partial U_{mi}}{\partial t} + \frac{\partial U_{mi} U_{mj}}{\partial x_j} = \frac{-1}{\rho_m} \frac{\partial P}{\partial x_i} + \nu_m \frac{\partial^2 U_{mi}}{\partial x_j \partial x_j} - \frac{\partial \overline{u'_{mi} u'_{mj}}}{\partial x_j} + g_i \tag{9}$$

where uppercase letters represent mean quantities and lowercase letters with primes represent fluctuating values, $\nu_m = \mu_m / \rho_m$, and where the products of ρ_m and the correlation terms $\overline{u'_{mi} u'_{mj}}$ are referred to as Reynolds' or turbulent stresses. Eq. 9 was obtained using Eq. 7b to estimate τ^t_{ij}. If viscous and turbulent stress terms are lumped into a single term, such as

$$\tau^T_{ij} = - \rho_m \overline{u'_{mi} u'_{mj}} + \mu_m \frac{\partial U_{mi}}{\partial x_j} \tag{10}$$

then the equation of motion can also be written as

$$\rho_m \frac{\partial U_{mi}}{\partial t} + \rho_m \frac{\partial U_{mi} U_{mj}}{\partial x_j} = - \frac{\partial P}{\partial x_i} + \frac{\partial \tau^T_{ij}}{\partial x_j} + \rho_m g_i \tag{11}$$

where τ_{ij}^{T} are the total stresses including viscous and turbulent components.

There are five energy equations useful in describing energy transformations in turbulent flows (Hinze, 1975). These are (1) conservation of total energy (total mechanical and heat), (2) total mechanical energy equation (mean and turbulent motion), (3) mechanical energy equation for mean motion, (4) mechanical energy equation for turbulent motion, and (5) thermal energy equation. Only the mechanical energy equation for mean motion will be given here.

The mechanical energy associated with the mean motion is obtained by using the dot product of the equation of mean motion (i.e., Eq. 9) and the mean velocity. This results in the following expression

$$\frac{\partial \frac{U_{mi}U_{mi}}{2}}{\partial t} = - \frac{\partial U_{mi} \{\frac{P}{\rho_m} + \frac{U_{mi}U_{mi}}{2}\}}{\partial x_i} - \boxed{\overline{(- u'_{mi} u'_{mj})} \frac{\partial U_{mi}}{\partial x_j}}$$

$$+ \frac{\partial U_{mi} \overline{(- u'_{mi} u'_{mj})}}{\partial x_j} + \nu_m \frac{\partial U_{mi} \{ \frac{\partial U_{mj}}{\partial x_i} + \frac{\partial U_{mi}}{\partial x_j} \}}{\partial x_j}$$

$$- \boxed{\nu_m \{ \frac{\partial U_{mj}}{\partial x_i} + \frac{\partial U_{mi}}{\partial x_j} \} \frac{\partial U_{mi}}{\partial x_j}} + U_{mi} g_i \qquad (12)$$

The two boxed terms are of major interest in Eq. 12. These two terms also appear in other energy equation with opposite signs. The first term

$$T_1 = \overline{- u'_{mi} u'_{mj}} \frac{\partial U_{mi}}{\partial x_j} \qquad (13a)$$

also appears in the mechanical energy equation for turbulent motion. It represents a lost in mechanical energy of mean motion and a gain in the mechanical energy of turbulent motion. The second term

$$T_2 = \nu_m \{ \frac{\partial U_{mj}}{\partial x_i} + \frac{\partial U_{mi}}{\partial x_j} \} \frac{\partial U_{mi}}{\partial x_j} \qquad (13b)$$

appears in the thermal energy equation. It represents a loss in mean mechanical energy and a gain in thermal energy as the result of viscous forces. Both T_1 and T_2 are energy dissipation rates per unit mass.

Energy dissipation rate

For the rill erosion model of this study, energy dissipation rate is defined as the rate in which mechanical energy of mean motion is lost either to viscous dissipation or to mechanical energy of turbulent motion. In the previous section, this rate per unit mass has

been defined by the two terms given in Eqs. 13a and 13b. Energy dissipation rate per unit volume can be written as

$$\phi_t = - \overline{\rho_m \, u'_{mi} \, u'_{mj}} \; \frac{\partial U_{mi}}{\partial x_j} + \mu_m \left\{ \frac{\partial U_{mj}}{\partial x_i} + \frac{\partial U_{mi}}{\partial x_j} \right\} \frac{\partial U_{mi}}{\partial x_j} \tag{14a}$$

where ϕ_t is the dissipation rate per unit volume. By using Eq. 10, ϕ_t can also be written as

$$\phi_t = \tau^T_{ij} \; \frac{\partial U_{mi}}{\partial x_j} \tag{14b}$$

where τ^T_{ij} is the total stress including viscous and turbulent components.

The total energy dissipation rate is defined by integrating Eq. 14b over the flow field, or,

$$\Phi_t = \int_{V_t} \tau^T_{ij} \; \frac{\partial U_{mi}}{\partial x_j} \, dV \tag{15}$$

where Φ_t is the total energy dissipation rate and V_t is the volume of the flow field of interest.

Following the approach given by Song and Yang (1980), it can be shown that, of the many possible Φ_t functions, the minimum function corresponds to the equation of motion for steady irrotational flows, assuming (1) no slip conditions at channel-fluid boundaries, (2) negligible τ^T_{ij} values at the fluid surface and planes normal to the flow direction, and (3) constant energy heads at the upstream and downstream points. Because of this solution, Eq. 15 provides a reasonable starting point for extrapolating to more complex flows.

Of course, the evaluation of Eq. 15 stills requires the estimation of τ^T_{ij} and $\partial U_{mi}/\partial x_j$.

Discussion

Energy dissipation rate is defined in Eq. 14b as the product of total stress and velocity gradient. Experimental data suggest that these two terms vary with suspended sediment load (Vanoni, 1946; Vanoni and Nomicos, 1960). Velocity gradients tend to increase with sediment load, whereas turbulent stresses tend to decrease. Energy dissipation rate can then either increase or decrease with sediment load depending on the relative changes in velocity gradient and total stress. This concept will be illustrated using the log velocity model.

The energy dissipation rate defined by Eq. 14b consists of nine different terms when expanded from its tensor notation. Using boundary-layer considerations, energy dissipation rate can be approximated as

$$\phi_t = \tau^T_{xy} \frac{\partial U_m}{\partial y} \tag{16}$$

where U_m is the mean mixture velocity in the x-direction, y is the vertical direction and τ^T_{xy} is stress associated with momentum transfer in the vertical direction.

The log velocity profile is based on the assumption of constant shear stress (Schlichting, 1979), or,

$$\tau^T_{xy} = \text{constant} = \tau_b = \rho_m gSh \tag{17a}$$

where τ_b is bed shear evaluated for a wide channel, g is gravity acceleration, S is slope and h is total flow depth. The log velocity profile has a velocity gradient defined as (Schlichting, 1979)

$$\frac{\partial U_m}{\partial y} = \frac{u_*}{\kappa y} = \frac{\sqrt{gSh}}{\kappa y} \tag{17b}$$

where u_* is shear velocity, κ is the von Karmon constant and y is a given height above the bed.

Using Eqs. 17a and 17b, the energy dissipation rate for sediment-free or clean flow can be written as

$$\phi_{tc} = \frac{\rho_f gSh_c \sqrt{gSh_c}}{\kappa_c y} \tag{18a}$$

and the energy dissipation rate for sediment-laden flows can be written as

$$\phi_{ts} = \frac{\rho_m gSh_s \sqrt{gSh_s}}{\kappa_s y} \tag{18b}$$

where the subscripts "c" and "s" refer to clean and sediment-laden flows, respectively.

For a given height above the bed, a lower dissipation rate for sediment-laden flows, compared to that of clean flows, occurs when $\phi_{ts} < \phi_{tc}$, or

$$\frac{h_s}{h_c} < \left[\frac{\rho_m}{\rho_f} \frac{\kappa_c}{\kappa_s} \right]^{2/3} \tag{19}$$

The right hand side of Eq. 19 is less than one. Important factors in determining whether energy dissipation rate increases or decreases are the ratios of h_s/h_c, ρ_m/ρ_f and κ_c/κ_s. For a given flow rate and slope, reduction in flow depth is possible for a change in its friction factor.

EVALUATION OF ENERGY DISSIPATION RATE

General formulation

Total energy dissipation rate is defined by Eq. 15. To simplify integration, an irregular shaped rill geometry is approximated by a trapezoidal rill shown in Fig. 1. This trapezoidal rill is defined such that the maximum flow depth, cross sectional area and top width are equal to that of the original rill. The shape shown in Fig. 1 is assumed to be representative of the geometry for the entire rill segment length. Following the general approach given by Keulegan (1938), integration with respect to y is always perpendicular to the bed. Only one-half of the rill area is directly integrated. The other half is obtained from symmetry.

Eq. 16 is evaluated by dividing the volume into bed and suspended zones identified in Fig. 1. The total energy dissipation rate can then be written as

$$\Phi_t = \int_{V_{sb}} \tau_{ij}^T \frac{\partial U_{mi}}{\partial x_j} dV + \int_{V_{ss}} \tau_{ij}^T \frac{\partial U_{mi}}{\partial x_j} dV \tag{20}$$

where V_{sb} is the volume of the bed zone and V_{ss} is the volume of the suspended zone. Different procedures are used to calculate the energy dissipation rate for each of these two zones.

Suspended zone

In the suspended zone, τ_{ij}^T is obtained from Eq. 11. For steady, irrotational flows this equation can be written as (Song and Yang, 1980)

$$\frac{\partial \rho_m g E}{\partial x_i} = \frac{\partial \tau_{ij}^T}{\partial x_j} \tag{21a}$$

where E is the total energy head defined as

$$E = \frac{U_{mj} U_{mj}}{2g} + \frac{P}{\rho_m g} + Y \tag{21b}$$

where Y is the distance above some datum height for a gravity potential field.

Following the approach given by Wilson and Barfield (1986), Eq. 21b can be simplified as

$$\frac{\partial \rho_m g E}{\partial x} = - \rho_m g S_e = \frac{\partial \tau^T{}_{xy}}{\partial y} \tag{22}$$

where S_e is the energy slope and y is in the vertical (depth) direction. Other stresses are assumed negligible.

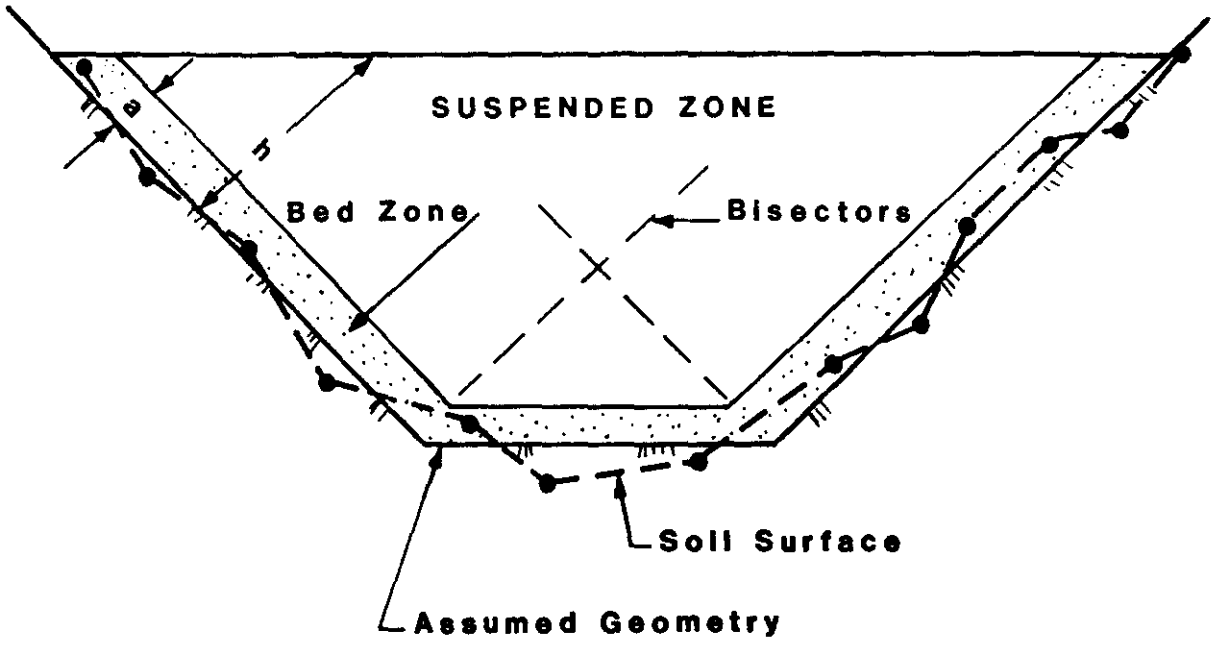

Figure 1. Idealized Rill Geometry for Evaluating Total Energy Dissipation Rate.

If the energy slope and mixture density are independent of depth, Eq. 22 can be integrated between the surface elevation to some point y, or,

$$\tau^T_{xy} = \rho_m g h S_e\left(1 - \frac{y}{h}\right) = \tau_b\left(1 - \frac{y}{h}\right) \tag{23}$$

where h is the flow depth and τ_b is the shear at the bed. Eq. 23 is often used in modeling turbulence in the suspended zone (Rouse, 1937; Vanoni, 1978; Wilson and Barfield, 1986).

The velocity gradient is approximated by using the log velocity profile previously given by Eq. 17b. Using Eqs. 16, 17b and 23, energy dissipation rate at any point in the flow can then be estimated as

$$\phi^s_t = \left[\frac{\rho_m g S_e h \sqrt{g S_e h}}{\kappa y}\right]\left[1 - \frac{y}{h}\right] \tag{24a}$$

and the total energy dissipation rate for the profile shown in Fig. 1 as

$$\Phi^s_t = \Delta x \left[\frac{\rho_m (g S_e)^{3/2}}{\kappa}\right] \int_0^{W_p} \int_a^h h^{3/2}\left[\frac{1}{y} - \frac{1}{h}\right] dy dz \tag{24b}$$

where ϕ^s_t and Φ^s_t are the energy dissipation rates at a point and for the flow, respectively, W_p is the wetted perimeter and a is the thickness of the bed zone. The thickness of the bed zone is taken as twice the diameter of the particles. Eq. 24b is evaluated numerically.

Bed zone

Energy dissipation rate in the bed zone is evaluated from the following equation

$$\Phi^b_t = \Delta x W_p \int_0^a \tau^T \frac{dU_m}{dy} dy = \Delta x W_p \int_{bed} \tau^T dU_m \tag{25a}$$

or as

$$\Phi^b_t = \Delta x W_p (\tau^T U_m)_{eff} \tag{25b}$$

where variations in stress and velocity gradient with space have been lumped into an effective shear and velocity product.

To evaluate Eq. 25b, it is assumed that effective shear can be divided into four possible components. One component is the viscous shear where the velocity of the surrounding fluid is essentiallly zero (no slip condition). Energy dissipation rate associated with this component is negligible. Another component is viscous and pressure drag on fixed particles extending into the flow. Energy dissipation rate is equal to a drag force multiplied by the velocity of its surrounding fluid. A third component is the forces necessary to keep moving

particles in motion, including forces to overcome solid-solid friction. Here energy dissipation rate is a function of friction forces and the relative velocity of particles. The fourth component is the forces required to accelerate detached particles. Energy dissipation rate for this component is estimated by the change in the kinetic energy of the eroded soil. Because of problems in evaluating forces and velocities associated with the first three components, their energy dissipation rates are lumped into a single expression.

Using this physical model, the energy dissipation rate is the bed zone is estimated as

$$\Phi_t^b = \Phi_e^b + \Phi_s^s \tag{26a}$$

where the subscripts e and s indicate energy dissipation rates for the eroded particles and remaining shear forces, respectively. Expressions to estimate these values are given as

$$\Phi_e^b = K_u^2 \, E_r^b \, \frac{u_*^2}{2} \tag{26b}$$

and

$$\Phi_s^b = K_\tau K_u W_p \Delta x u_* \tau_b' \tag{26c}$$

where E_r^b is bed erosion rate, u_* is shear velocity, τ_b' is a bed shear (adjusted for the force used in Eq. 25b), $K_u u_*$ is an effective velocity in the bed zone, K_u is a velocity constant, and K_τ is a constant to account for different energy dissipation rates among the three possible components incorporated in Eq. 26c.

DETACHMENT AND TRANSPORT ALGORITHM

Introduction

The algorithm differs from other minimization approaches (Yang, 1976; Chang and Hill, 1977; Chang, 1979, 1982b, 1984a, 1984b, 1985) in that it does not use an empirical transport equation. Energy dissipation rate is minimized with respect to suspended sediment load. Constraints are the conservation of mass of both sediment and water components, conservation of force-momentum for water component, and the detachment rate of the soil.

The model assumes a single representative particle size and neglects lateral inflows. If the minimization principle proves useful, the algorithm can be easily expanded and tested on more complex problems. A simplified flow chart of the model is shown in Fig. 2. Each of the key components in the algorithm will be described separately.

Rill geometry

Geometry characteristics are necessary to estimate flow area, hydraulic radius and top width which are used in routing water downslope and calculating energy dissipation rates. For each rill segment, the cross sectional profile is approximated by linear piecewise polynomials as shown in Fig. 3a. Linear piecewise polynomials were selected because they can represent highly irregular profiles and are relatively easy to manipulate. It is from this representation that the idealized rill geometry given in Fig. 1 is calculated.

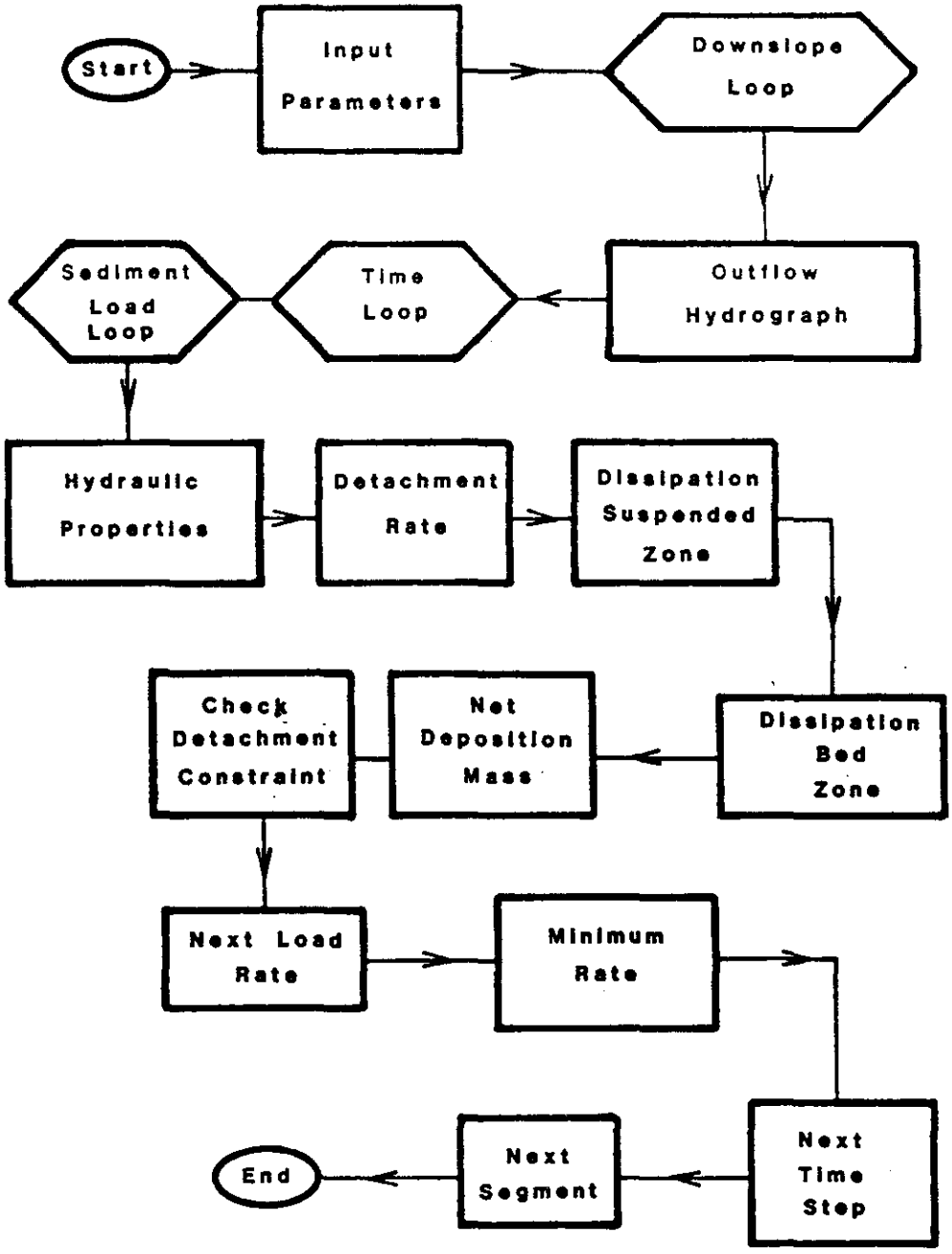

Figure 2. Flow Chart for Erosion Model.

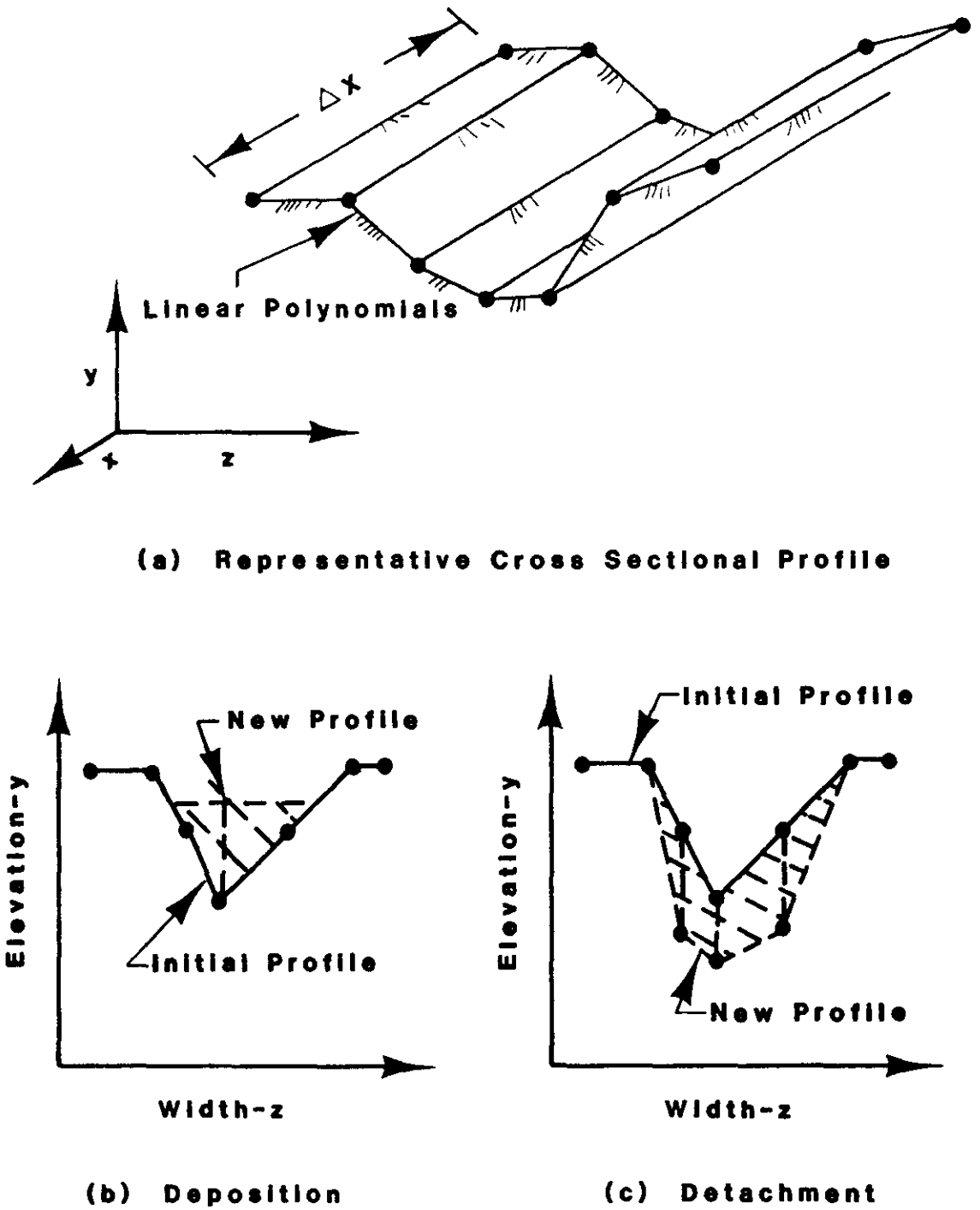

Figure 3. Rill Geometry Represented by (a) Linear Line Segments and Changes Due to (b) Deposition and (c) Detachment.

Rill profiles are allowed to change with time as the result of detachment or deposition. Schematics illustrating these changes for deposition and detachment are shown in Fig. 3b and Fig. 3c, respectively. During deposition, the sediment is assumed to be deposited in horizontal layers. During detachment, the profile is modified based on the area detached between breakpoints of the piecewise polynomials. Procedures used to estimate detachment rates will be given later.

Outflow hydrograph

Total flow in the rill is divided into water and sediment components. The outflow rate of water is estimated independently of the sediment load rate using a modified form of Dooge et al.'s (1982) Muskingum flood routing method. This method is based on a linearized form of the St. Venant equation and, hence, maintains a rough balance between forces and momentum. Ruffini and Wilson (1985) have shown that Dooge et al.'s method accurately approximates the results obtained using the full St. Venant equations.

Sediment load rate

Energy dissipation rate is minimized with respect to sediment load rate. Suspended sediment is varied from clean flow to a maximum value determined by detachment capacity using a constant step size of 5 gm/s. For each load rate, hydraulic properties of the flow are calculated and the energy dissipation rates are estimated. The minimum value is then estimated by a second degree polynomial fitted to points surrounding the lowest predicted dissipation rate (Beveridge and Schechter, 1970).

Bed load rate is calculated directly from the suspended sediment load assuming identical concentration at their interface. Bed load rate is estimated as

$$q_{sb} = g_c q_{ss} \tag{27a}$$

where q_{sb} and q_{ss} are the sediment load rates in the bed and suspended zone, respectively, and g_c is a function to match concentration values between the two zones. A number of equations have been developed for g_c (see Simons and Senturk, 1976). The following equation is used here,

$$g_c = \frac{(11.6)au_*}{hU_m} \tag{27b}$$

where U_m is a velocity and other terms are as previously defined. Eq. 27b is roughly equal to Einstein's (1950) equation for a small ratio of settling velocity to shear velocity.

Variation in hydraulic characteristics

Hydraulic properties have experimentally been observed to change with sediment as the result of changing bed form resistance and von Karmon constant (Simons and Senturk, 1976). Changes in the von Karmon constant is predicted using the curve shown in Fig. 4. This figure shows observed variations in von Karmon constant for a dimensionless energy rate ratio, which is defined roughly as the power (rate of energy expenditure) to support suspended sediment to the power to overcome frictional forces (Simons and Senturk, 1976). Mathematically, this ratio is defined as

$$P^* = \left(\frac{\rho_s - \rho_f}{\rho_f}\right) \left(\frac{\omega_s c}{U \sin\alpha}\right) \tag{28}$$

where P^* is a dimensionless power term used in Fig. 4, ω_s is the settling velocity of the particle, c is volumetric concentration, α is the slope angle and U is a mean velocity.

Fig. 4 clearly shows a general trend for von Karmon κ to decrease with increasing P^*. This effect was predicted by fitting a cubic spline to the curve given in Simons and Senturk to represent the observed data.

As shown by Eq. 19, changes in flow depth are also important is determining energy dissipation rates. In the rill erosion model, this change is predicted by adjusting Manning's n. The general approach of Keulegan (1938) will be modified to estimate a new Manning's n for a change in von Karmon constant.

Keulegan (1938) showed that Manning's equation could be evaluated from the log velocity profile. Manning's equation can be written as

$$\frac{\overline{U}}{u_*} = C \left[\frac{R}{K_s}\right]^{1/6} \tag{29a}$$

where $\overline{U}$ is the mean velocity, R is the hydraulic radius, K_s is the effective roughness and C is a constant defined as

$$C = \frac{K_s^{1/6}}{n \sqrt{g}} \tag{29b}$$

where n is Manning's n.

The log velocity profile can be written as Keulegan (1938)

$$\frac{\overline{U}}{u_*} = 6.25 + \frac{1}{\kappa} \ln\left(\frac{R}{K_s}\right) \tag{29c}$$

where κ is von Karmon constant.

Setting Eqs. 29a and 29c equal to each other, the following expression can be obtained

$$C \left[\frac{R}{K_s}\right]^{1/6} = 6.25 + \frac{1}{\kappa} \ln\left(\frac{R}{K_s}\right) \tag{30}$$

By numerically evaluating C for a large range of R/K_s values, C is found to be relatively constant, and an average value for six points is used to obtain

$$C = 2.396 + \frac{2.161}{\kappa} \tag{31}$$

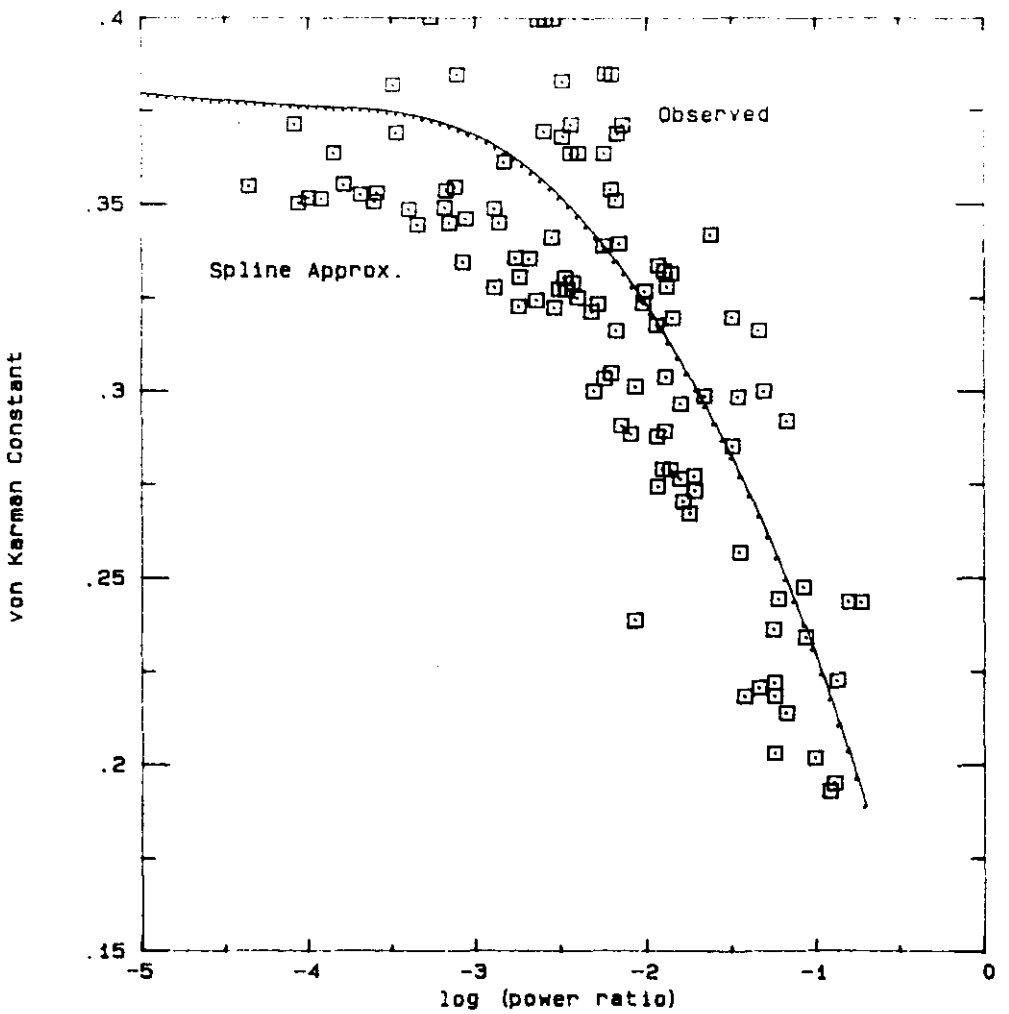

Figure 4. Effects of Sediment of the von Karman Constant
(Modified from Simons and Senturk, 1976)

Finally, by examining the ratio of C with clean water to C with sediment-laden water, the following relationship is obtained

$$n'_s = n_c \left[\frac{8\kappa_s}{2.4\kappa_s + 2.2} \right] \tag{32}$$

where n_c is Manning's n for clean water flows, n'_s is Manning's n adjusted for a change in the von Karmon constant and κ_s corresponds to von Karmon constant for sediment-laden flows. Eq. 32 is developed assuming that the von Karmon constant for clean water is 0.385.

Eq. 32 provides an estimate of Manning's n for different von Karmon constants. Manning's n may also depend on bed roughness factors. These factors are difficult to predict. In the rill erosion model, Manning's n for sediment-laden flows is predicted using the general form

$$n_s = f(c) n'_s \tag{33a}$$

where

$$f(c) = K_{f1} \exp(- K_{f2} c) \tag{33b}$$

where n_s is Manning's n for sediment-laden flows, c is concentrations, and K_{f1} and K_{f2} are constants. f(c) is a function to vary n'_s for bed roughness factors. Alternatively, f(c) can also be viewed as an adjustment for approximation errors in Eq. 32.

Detachment

Detachment rate is used to (1) determine the energy dissipation rate in the bed zone (i.e., Eq. 26b) and (2) provide a maximum load rate constraint for flow in the suspended zone (i.e., increase in suspended load can not exceed its supply). The potential detachment rate is predicted using the following general equation (Foster, 1982)

$$E_p = K_e(\tau_b - \tau_c) \tag{34}$$

where E_p is the potential detachment rate, K_e is a soil erodibility constant, τ_b is the bed shear and τ_c is the critical shear. Bed shear is allowed to vary with location on the rill boundary using the equation given by Foster (1982).

Total detachment rate decreases as the erodible surface area becomes smaller. Erodible surface area is assumed to decrease with the number of particles moving in the bed layer. Actual detachment rate is estimated as

$$E_r^b = E_p \left(1 - \frac{q_{sb}}{q_{sb}^*}\right) \tag{35}$$

where E_r^b is the detachment rate, q_{sb} is the bed load rate and q_{sb}^* is a maximum bed load rate.

Maximum bed load rate is estimated using the movement of a layer of particles at a maximum packing density and traveling at the bed velocity.

Deposition

Net deposition of sediment is calculated using mass balance relationships for both the suspended and bed zones. Advected mass in the bed zone is neglected. A negative deposition corresponds to detached sediment mass.

METHODOLOGY: EXPERIMENTAL

LABORATORY STUDIES

Erosion table

To study the interactions between the transport of eroded soil, the flow rate, and rill geometry, a relatively large-scale laboratory apparatus was constructed in one of the Agricultural Engineering Department's research shops at the edge of the Oklahoma State University campus. Erosion processes can be studied on 2.4 m by 9.8 m (8 ft x 32 ft) surface. To simulate longer upland flow segments, sediment-laden flows can be entered at the inlet of the table. Clean water and sediment-laden flows can be mixed at this point and allowed to flow onto the plot. To obtain different slopes, two false floors are placed under the erosion surface and hinged so that upslope floor can rotate to different angles. A wet laboratory is adjacient to the erosion table for use in the analysis of runoff data.

A view of the erosion table from the upslope end of the plot is shown in Fig. 5. The instrumentation rack and rainfall simulator are shown on this print. The instrumentation rack is part of the system used to measure geometric characteristics of rill flows and is discussed in the next section. The rainfall simulator was not used in this study. Additional details about the design and operation of the erosion table are given by Wilson and Rice (1987).

Measurement of geometry characteristics of rills

As part of this study, an efficient and accurate instrumentation technique was developed to measure rill geometries using relatively low-cost image processing equipment and structured lighting concepts. A three dimensional schematic of our system is shown in Fig. 6. A laser source projects a well-defined stripe of light which in Fig. 6 intercepts a block of fixed height situated on a flat surface. The light is gathered through a lens and focused on a sensor located behind the lens. The sensor image of the striped light is shown in the inset of Fig. 6. The image is digitized into a square grid (512 x 512) of discrete picture elements or pixels. Since the light is striking the block at an angle, there is a difference in pixel locations between the top of the block and that of the flat surface. Differences in these locations can be used to determine elevation.

The laser and camera components of the system are supported and moved over the erosion table surface using the instrumentation rack shown in Fig. 5. Movement in the x, y and z directions is powered by three stepper motors controlled by an IBM PC-AT. Motion in the y and z directions is obtain using precision racks and pinions and in the x direction using a chain driven system.

Output signals from the camera are sent to a Data Translation DT-2851 frame grabber board located in an IBM PC-AT. This board has flashed A/D converters that can digitize a frame in 1/30 of a second. Its resolution is 512 lines by 512 pixels with 256 possible gray values. Limited processing on the board can be done such as frame averaging, frame addition and subtraction, and windowing. The computational speed of the system is increased using a Data Translation DT-2858 auxiliary frame processor board. This board has high speed direct interface to the frame grabber memory, has pipelined arithmetic performance, and supports NxM convolutions, frame averaging, normalization and histograming operations.

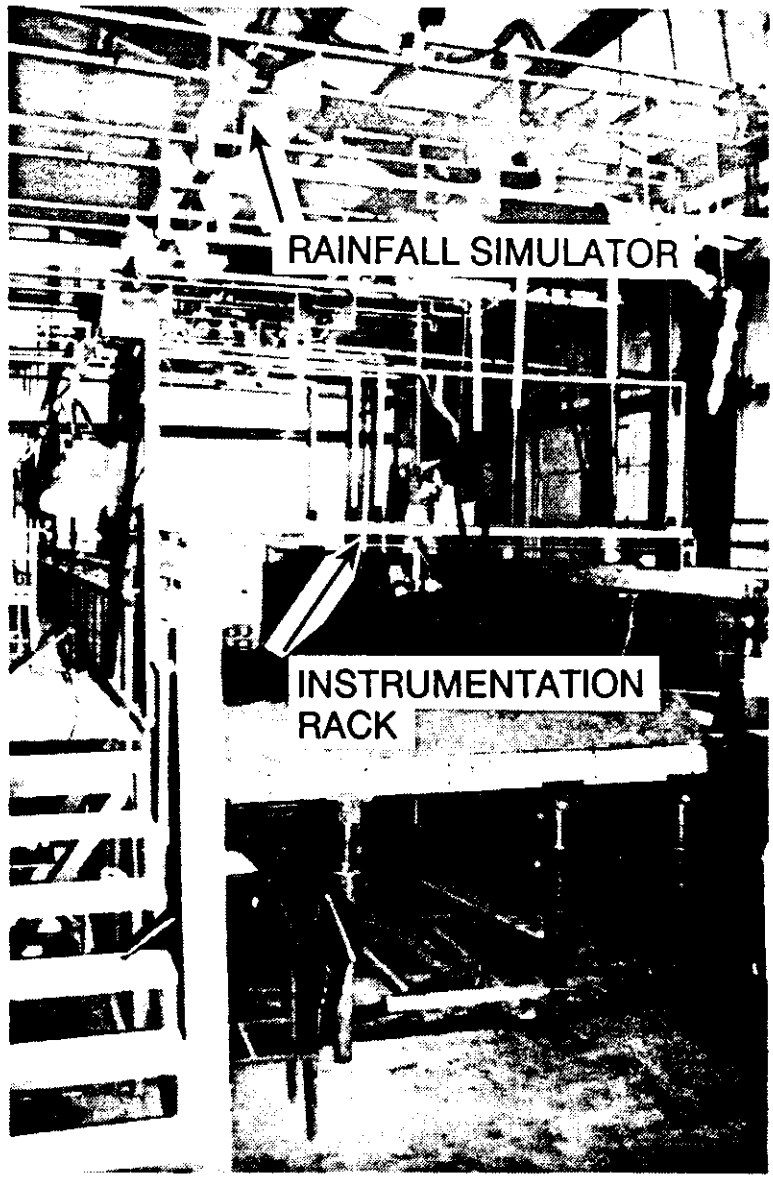

Figure 5. Downslope View of Erosion Apparatus.

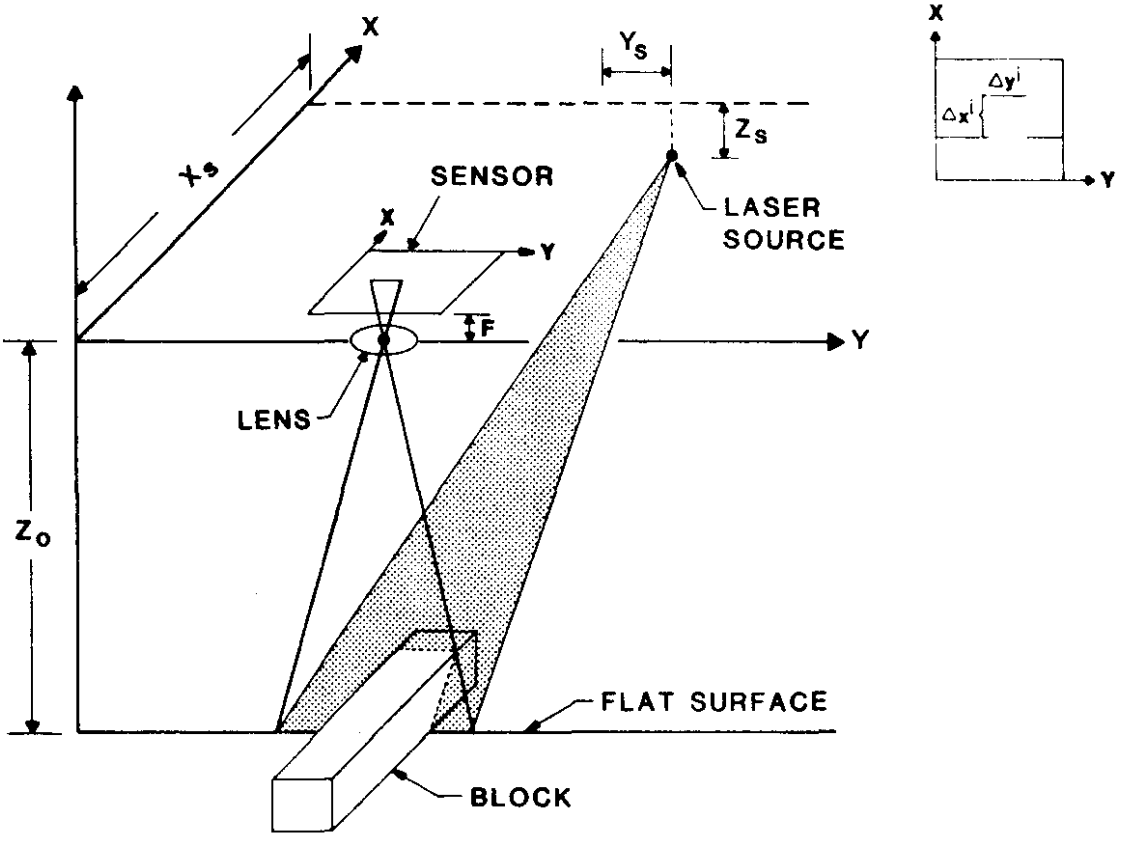

Figure 6. Schematic Illustrating Structured Lighting Concepts.

Software has been written to manipulate and analyze the images. A critical algorithm is identifying the location of the laser line. The key components of this algorithm are (1) enhancing the image using a convolution filter, (2) selecting the appropriate gray level and (3) determining the midpoint of the line. The system can measure 300 data points in less than six seconds. Theoretical and operational details and calibration procedures are given by Rice et al. (1987a, 1988).

Two sets of experiments were conducted to evaluate the accuracy and applicability of structured lighting techniques for measuring surface profiles. The first set of experiments used "precision", rigid objects. These objects were constructed precisely and represented well-defined shapes for evaluating accuracy. The second set of experiments used soil with pre-formed surface depressions to test the applicability of the system.

A summary of the measured heights for five square tubing blocks are given in Table 1. Eight different measurements were taken for each block at various camera heights as discussed by Rice et al. (1987a, 1988a). The mean values is within 0.1 mm of the actual value for each height. The maximum error for rigid blocks was only 0.63 mm. No noticeable problems were found using the system on soils. The measured values for soils were within the accuracy of the commonly used pin displacement method. Details of these results are also presented by Rice et al. (1987a, 1988a).

Table 1
Summary of Height Measurements

Block	Actual Height (mm)	Mean Value (mm)	Std Dev. (mm)
#1	12.80	12.84	0.128
#2	25.04	24.95	0.128
#3	37.69	37.60	0.196
#4	50.37	50.31	0.119
#5	62.08	62.02	0.082

Finally, dynamic changes in the top width of rills during the event are also obtained using image processing techniques. Here a solid-state video camera is located directly over a rill and records the rilling processes. Images are analyzed using Data Translation's DT-2851 and DT-2858 image processing boards. Since the gray level of flowing sediment-laden water is different than the surrounding soil, it is possible to locate the interface boundaries between them. It is then relatively easy to measure the top width at different times using image processing software.

Measurement of surface velocities in rills

In addition to the development of instrumentation techniques to measure rill geometry, unique techniques were also developed to measure near-surface velocities of rill flows. Surface velocities are determined by the movement of small wooden beads as they float past a camera. Image processing techniques were used to determine the travel distance within a known time interval and hence surface velocities. Details of the procedure are given by Rice et al. (1987b, 1988b).

Different algorithms were developed for slow and fast water velocities. Both algorithms determined the location of beads with time using a connectivity analysis given by Cunningham (1981). For the slow water algorithm, the time interval between beads was obtained by evaluating different image frames, whereas the fast water algorithm used a single frame to trace the movement of beads. Velocity is obtained directly from the

measured displacement distance over a given time interval.

Two sets of experiments were conducted to evaluate the accuracy and applicability of the velocity measuring algorithms. The first set of experiments used beads glued to a rotating belt to provide a well-defined, known velocity. The second set of experiments was used to test the applicability of the system to open channel flows. In both sets of tests, the image processing velocities corresponded very well to observed values. The results for open channel flows are summarized in Fig. 7. The accuracy of the system was estimated as $\pm$ 10 mm/s. Additional experimental details are given by Rice et al. (1987b, 1988b).

Experimental design for laboratory studies

Laboratory experiments were conducted to study interactions among transport rate and flow and geometry characteristics and to evaluate minimum rate of energy dissipation concepts. Preformed rills were constructed in the erosion table using a specially constructed tool attached to a John Deere 318 tractor. The initial rill geometry was approximately parabolic with dimensions corresponding to that reported by Rohlf and Meadows (1980) and Line and Meyer (1987) for observed rills. A local loam soil (38% sand, 40% silt and 22% clay) was used in the study.

Data were gathered for two different slopes of 2% and 8% and for two levels of inflow concentration. Two replicates were used to obtain a total of eight runs. Prior to each run, the soil was roto-tilled; a rill was then formed and saturated using a drip hose. Three different inflow rates were used for each run: (1) low flow rate of roughly 0.2 l/s for the first fifteen minutes, (2) medium flow rate of roughly 0.5 l/s for next fifteen minutes, and (3) high flow rate of roughly 1.0 l/s for the last fifteen minutes. A small break was allowed between flow rates so that rill profiles could be measured.

During each run, the volumetric flow rate and effluent concentration were recorded at the outlet of the rill. At roughly the midpoint between inlet and outlet of the rill (distance of 5 m downslope) surface velocities and rill top widths were recorded using procedures previously discussed. Rill profiles were measured at fifteen upslope locations at equal spacing of 0.05 m before and after the run using structured lighting techniques. In addition, intermediate profiles were taken at three locations of equal spacing of 0.1 m between the different flow rates. Bulk densities were taken in the rills following the runs.

FIELD STUDIES

The final phase of this project was to obtain data in the field. This step required the construction of a portable, field rainfall simulator. A portable rainfall simulator was designed and constructed similar to that built by Dickey et al. (1984). The main advantages of this particular type of simulator were its portability and relatively low construciton costs. It has a rotating boom simulator capable of spraying an area roughly 14 feet by 35 feet. Image processing techniques developed in the laboratory for measuring rill profiles were extended to the field.

Field erosion studies were conducted at an Agricultural Engineering Departmental site located just off campus. Here the emphasis was to measure the shape of rills generated from runoff. A suitable site was cleared of its vegetation. Rainfall was applied to the plot until rills of significant size were formed. The profiles of these rills were then measured.

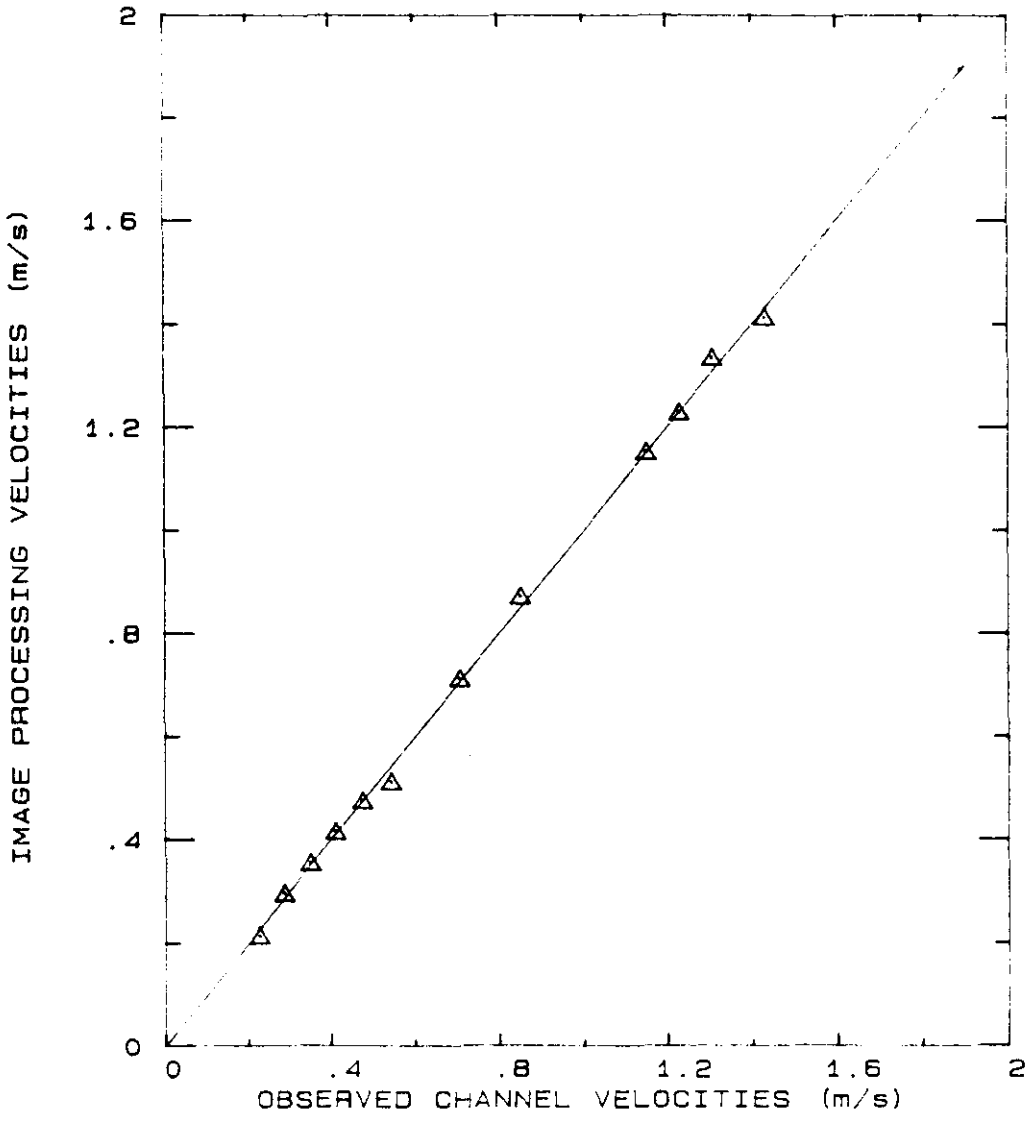

Figure 7. Comparison of Channel and Image Processing Velocities.

FINDINGS

LABORATORY STUDIES

Observed data

The sedimentologic response of the preformed rills was strongly dependent on slope. For the eight percent slope, the average detachment rates for clean water runs were 0.17 gm/m/s for the low flow rate, 0.72 gm/m/s for the medium flow rate and 2.26 gm/m/s for the high flow rate; whereas for the clean water, four percent slope runs the corresponding average detachment rates were 0.04, 0.21, and 0.79 gm/m/s for the low, medium and high flow rates, respectively. Detachment rates at the eight percent are three to four times larger than those observed at four percent. These ratios also correspond roughly to observed ratios of transport rates at the outlet of the rill.

Observed sedimentologic response was also dependent on the sediment concentration at the inlet of the rill. For the eight percent slope, the average detachment rates of sediment-laden runs were 0.03, 0.0 (no net detachment) and 0.53 gm/m/s for the low, medium and high flow rates, which are at least four times smaller than values given in the previous paragraph. For the four percent slope, the effects of non-zero influent concentration were not as significant resulting in average detachment rates of 0.03, 0.03 and 0.77 gm/m/s for each of the three flow rates. Lower influent concentration values were used in the four percent runs. A reduction in net detachment rate was expected as the transport rate approached its maximum capacity.

The effects of inlet sediment concentration on near-surface velocities are not clear. For the eight percent slope, there was consistent trend for larger velocities with the sediment-laden runs. The averaged surface velocities for clean water runs were 0.92, 1.14 and 1.26 m/s for the low, medium and high flow rates, respectively; whereas, the corresponding velocities for the sediment-laden runs were 1.15, 1.48 and 1.85 m/s. For the four percent slope, however, a slightly opposite trend appeared to occur, that is, smaller velocities for the sediment-laden runs. Here the data were not as consistent in the eight percent runs. The averaged surface velocities for clean water runs were 0.79, 0.91 and 0.98 m/s for the low, medium and high flow rates, respectively; whereas, the corresponding velocities for the sediment-laden runs were 0.65, 0.89 and 0.96 m/s. In all of these calculations the velocities were adjusted to a standard flow rate assuming linear relationships.

The detachment rate in the rills was highly variable, especially for the eight percent runs. Before and after profiles for two locations along the rill are shown in Fig. 8. The two profiles were 0.2 m apart. The detached mass per unit length for the downslope profile was roughly 13 gm/cm compared to 131 gm/cm for the upslope profile. Uniform flow conditions assumed in the proposed model (and most other models) did not occur. Small perturbations in the rill slope often resulted in an overfall condition. The movement of this overfall appeared to be an important component in the erosion process.

Comparisons with predicted values

Procedures and assumptions for determining parameters for the detachment and transport model are as follows:

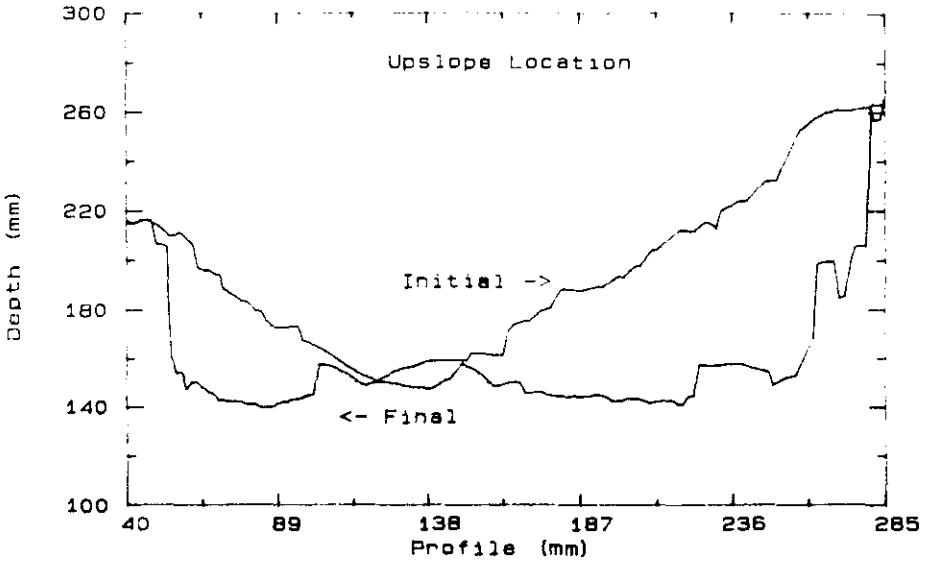

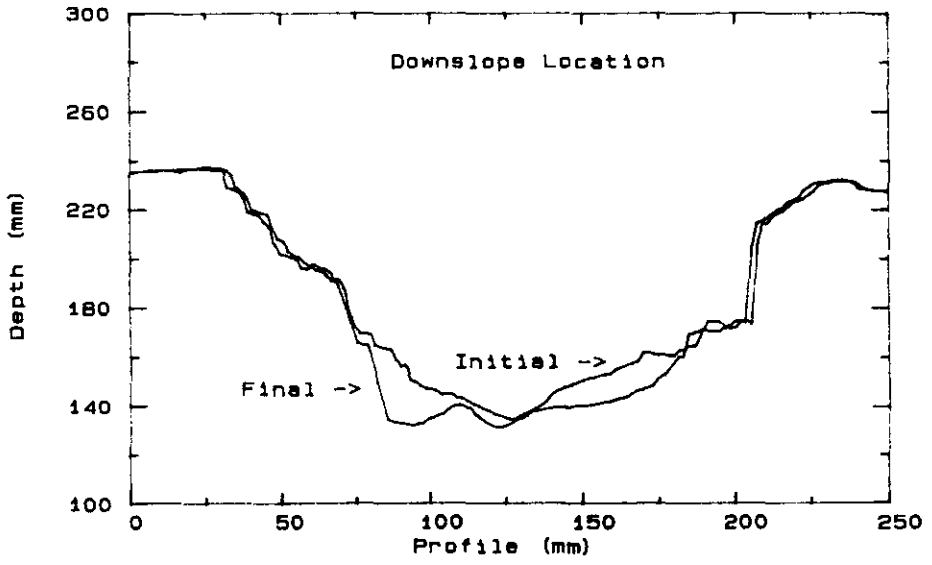

Figure 8. Spatial Variability of Detachment.

(1) The rill was modeled as a single segment. Representative cross-sectional area, velocity and top width were determined by data at roughly the midpoint of the rill.

(2) The observed cross-section before the each flow rate was approximated by a parabolic profile to simplify calculations matched to the observed data.

(3) From observed flow width and parabolic profile, the flow depth, hydraulic radius and wetted perimeter were calculated.

(4) Using the measured water surface slope (S) and calculated hydraulic radius (R), the average bed shear (τ) was estimated as ρgSR and the shear velocity as the square root of gSR.

(5) Measured surface velocities were converted to mean velocities using the relationships developed by Rice et al. (1987b).

(6) Manning's n was then estimated.

(7) Observed detached mass per unit length using measured influent and effluent concentrations was divided by the wetted perimeter to determine E_p in Eq. 34.

(8) Critical shear value was assumed equal to zero. Soil erodibility constant in Eq. 34 can then be approximated by dividing E_p by the bed shear.

(9) Representative particle size was taken as the value corresponding to the fifty percent finer from observed distributions.

(10) The following values were assumed: $K_u = 1$, $K_\tau = 0.5$, $K_{f1} = 1$ and $K_{f2} = 0$.

Predicted and observed transport rates are shown in Table 2 for the clean water runs. The observed values varied considerably with flow rates and slopes. The predicted transport rates, however, have either an almost constant value of 7 gm/s or sediment-free water. There was a slight trend for predicted transport rate to increase with flow rate. Predicted transport rate was not dependent on slope.

It is unclear whether these poor predictions are caused by an erroneous theoretical hypothesis, that is that rills minimize their energy dissipation rates, or by an oversimplified algorithm which was required to implement the hypothesis. This issue will be addressed by conducting a sensitivity analysis of key input parameters in the next section. Results are presented separately for bed and suspended zone parameters.

Sensitivity of predicted values

All sensitivity runs were conducted for a triangular shaped rill of 1:1 sideslopes and length of 2 m. Constant volumetric flow rate, slope, particle diameter and critical shear stress were set at 1000 cc/s, 0.05, 0.0012 cm and 1 N/m/m, respectively.

Table 2
Predicted and Observed Transport Rates

Slope	Site	Flow Rate	Transport Rate Predicted (gm/s)	Transport Rate Observed (gm/s)
		Low	0.0	1.8
8	1	Med	7.3	8.5
		High	7.5	17.6
		Low	7.0	1.0
8	2	Med	7.4	3.2
		High	7.5	17.2
		Low	7.2	0.3
4	1	Med	7.4	2.6
		High	7.5	10.0
		Low	0.0	0.3
4	2	Med	0.0	1.2
		High	0.0	4.2

The sensitivity of energy dissipation rate was evaluated by varying constants K_u (effective bed velocity), K_τ (effective bed shear) and K_e (soil erodibility factor). The effective bed velocity was varied between 0.2 and 6.0, effective bed constant was varied between 0.1 and 0.75, and soil erodibility factor was varied between 1.0 and 10.0 gm/N. The resistance constants of K_{f1} and K_{f2} were set equal to one and zero, respectively.

Overall the variation in bed parameters over this range of values had little influence on locating the minimum energy dissipation rate. This is because the contribution of bed energy dissipation rate is relatively small in comparison to dissipation rate in the suspended zone. Predicted energy dissipation rates for the bed zone and total flow are shown in Fig. 9. These results were obtained using K_u=1, K_τ=0.5, and K_e=5.0.

In addition to its relatively small contribution to total dissipation rate, bed dissipation rate is dominated by "shear" rate given by Eq. 26c. Since the dissipation rate in the suspended zone is also strongly dependent on τ_b, load rate corresponding to minimum dissipation rate in the bed zone is approximately equal to the suspended zone minimum value. Therefore, the bed zone only accentuated results obtained in the suspended zone.

The sensitivity of energy dissipation rate in the suspended zone was evaluated using different von Karmon constants (i.e., Fig. 4) and for variations in Manning's n due to the function f(c) in Eq. 33a. The von Karmon curves were modified by linearly increasing or decreasing predicted values of Fig. 4. Manning's n was varied using K_{f1}=1 and K_{f2}=10. Bed parameters of K_u, K_τ, and K_e were set to 1, 0.5, and 5 gm/N, respectively.

The effects of varying von Karmon values $\pm$ 5% over the range of power ratio had a relatively minor effect on the location of the minimum dissipation rate. A positive change

shifted the location to larger sediment rates, whereas a negative change shifted the location to smaller sediment rates.

The results of changing Manning's n were, however, quite important. In Fig. 10, the energy dissipation rate is shown for the case when the function f(c)=1 (i.e., K_{f1}=1; K_{f2}=0). As shown by this figure, the minimum value is 4.6 gm/s, which is close to clean water. Also shown on the figure are the results for K_{f1}=1 and K_{f2}=10. For this condition, the minimum value corresponded to detachment limiting value of > 50 gm/s, which the largest concentration that can be achieved for the given detachment rate. Variation in Manning's n over this range, due to f(c), was less than 20 percent. Therefore, a relatively minor change in Manning's n varied the sediment load from relatively clean to relatively "dirty" flows. Since an accurate estimate of f(c) is difficult, this is a major limitation of the proposed model. Improved procedures are needed in estimating this effect before the minimum rate of energy dissipation hypothesis can be evaluated more thoroughly.

FIELD STUDIES

A typical rill profiles gathered in the field study are shown in Fig. 11. These three profiles are gathered on the same rill and can be used to illustrate rill development. At the upslope point, the rill is relatively shallow. As the flow increases downslope, the rill becomes deeper and wider.

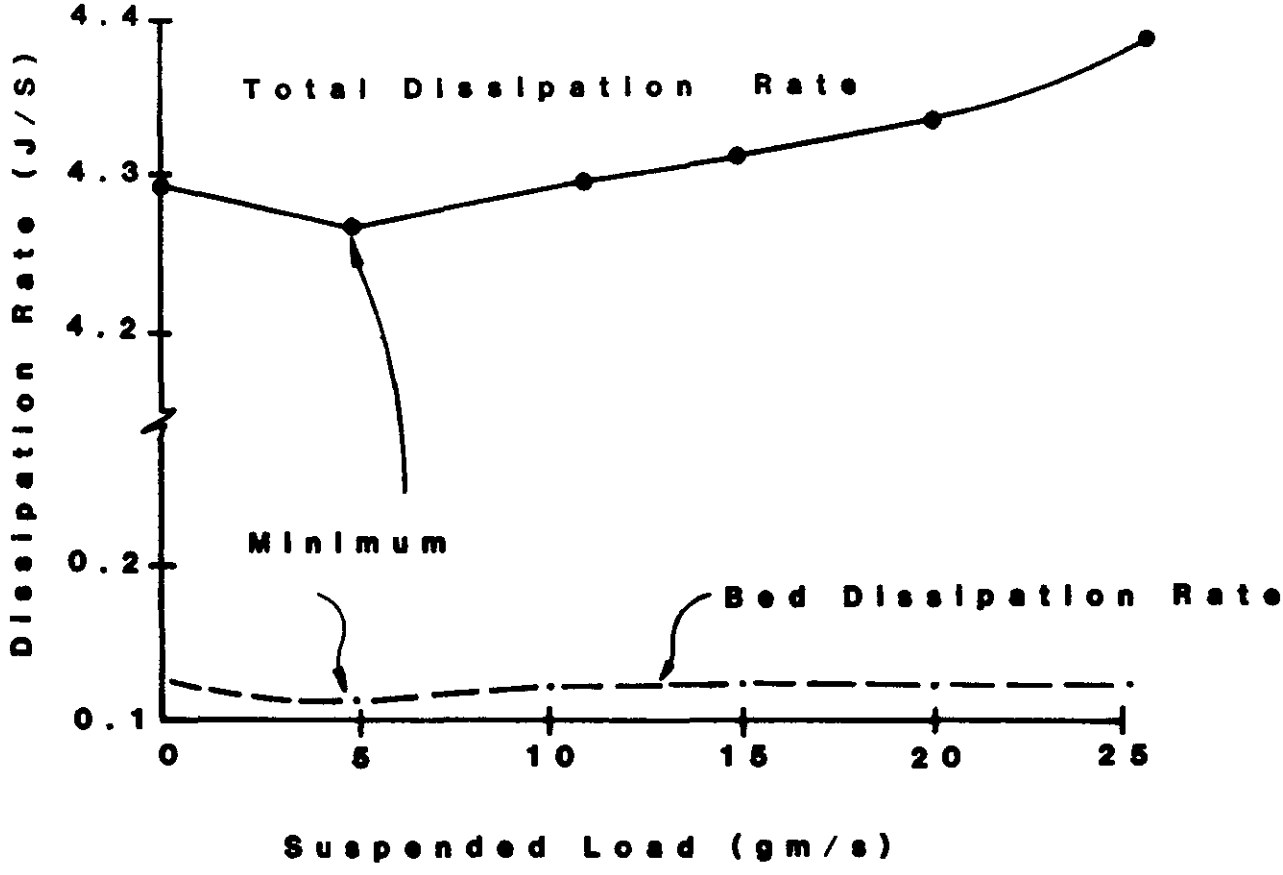

Figure 9. Total and Bed Energy Dissipation Rates.

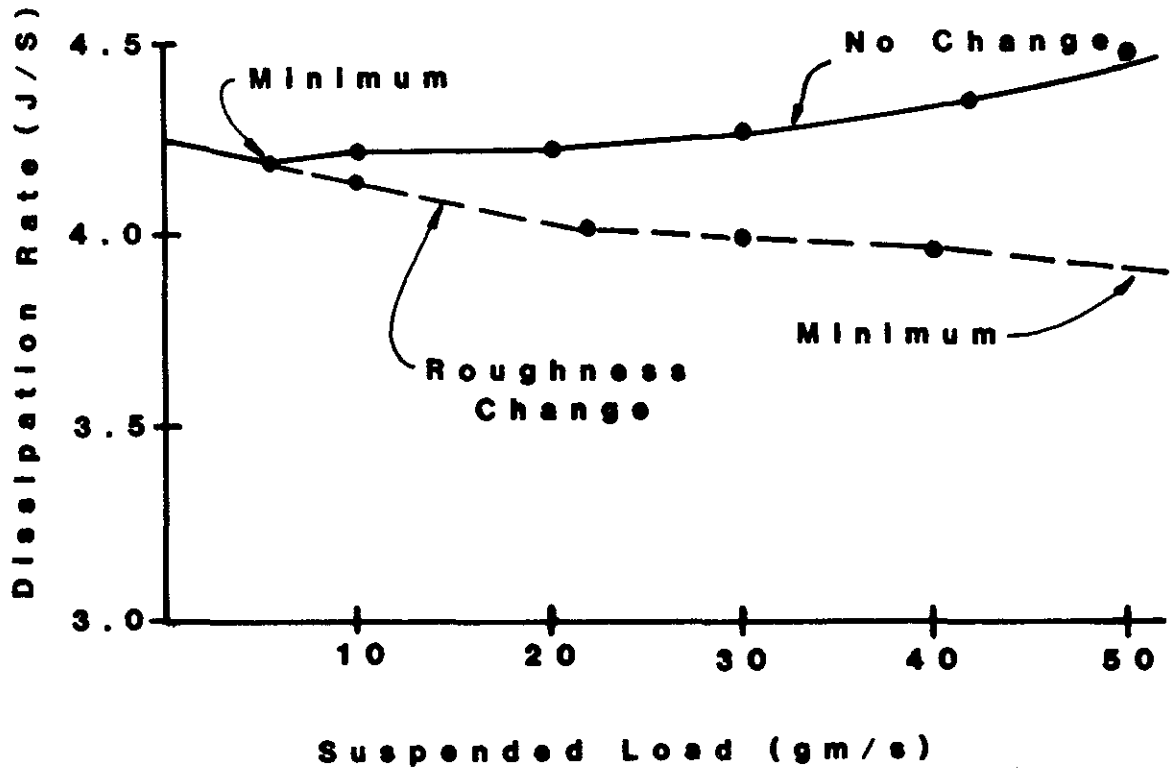

Figure 10. Sensitivity of Dissipation Rate on Bed Roughness.

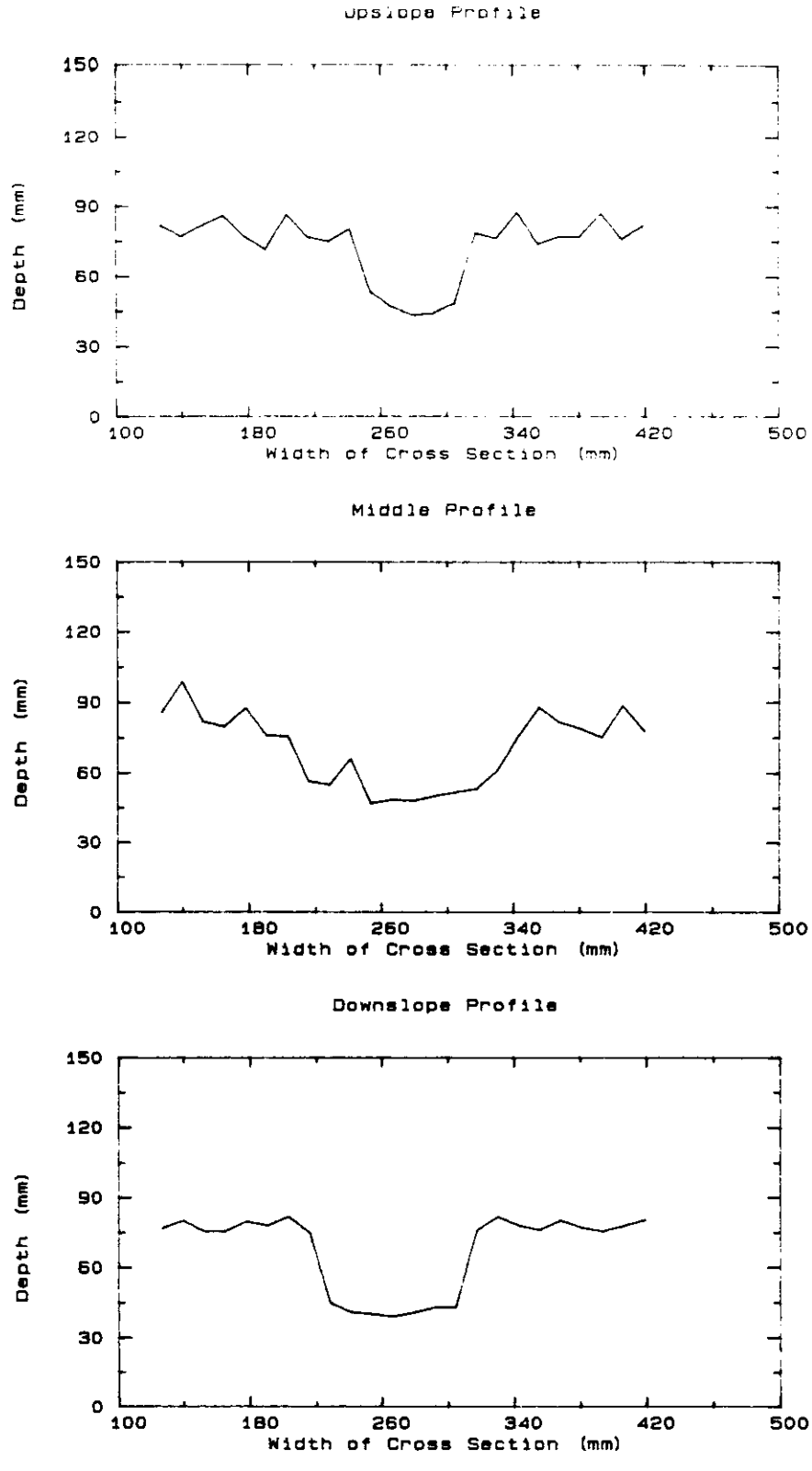

Figure 11. Observed Profiles in Field Study.

BIBLIOGRAPHY

Bagnold, R. A. Experiments on a gravity-free dispersion of large solid spheres in a Newtonian fluid under shear. Proc. Royal Soc., Ser. A, Vol. 225:49-63, 1954.

Bagnold, R. A. The flow of cohesionless grains in fluids. Royal Society London Phil. Trans. Ser. A., No. 964, Vol. 249: 235-297, 1956.

Batchelor, G. K. and J. T. Green. The determination of the bulk stress in a suspension of spherical particles to order c2. J. Fluid Mech., Vol. 56(3):401-427, 1972.

Beveridge, G. S. G. and R. S. Schechter. Optimization: Theory and Practice. McGraw-Hill Book Company, New York, 1970.

Brebner, A. and K. C. Wilson. Derivation of the regime equations from relationships for pressurized flow by use of the principle of minimum energy-degradation rate. Proc. Inst. Civil Eng., Vol. 36:47-62, 1967.

Buyevich, Yu. A. and I. N. Shchelchkova. Flow of dense suspensions. Aerospace Sci., Vol. 18:121-150, 1978.

Chang, H. H. Geometry of rivers in regime. J. of the Hydraulics Div., Proc. of the American Soc. of Civil Engineers, Vol. 105(HY6):691-706, 1979.

Chang, H. H. Mathematical model for erodible channels. J. of the Hydraulics Div., Proc. of the American Society of Civil Engineers, Vol. 108(HY5):678-687, 1982a.

Chang, H. H. Fluvial hydraulics of deltas and alluvial fans. J. of the Hydraulics Div., Proc. of the American Society of Civil Engineers, Vol. 108(HY11):1282-1295, 1982b.

Chang, H. H. Analysis of river meanders. J. of Hydraulic Engineering, Vol. 110(1):37-50, 1984a.

Chang, H. H. Modeling of river channel changes. J. of Hydraulic Engineering, Vol. 110(2):157-172, 1984b.

Chang, H. H. Water and sediment routing through curved channels. J. of Hydraulic Engineering, Vol. 111(4):644-658, 1985.

Chang, H. H. and J. C. Hill. Minimum stream power for rivers and deltas. J. of the Hydraulics Div., Proc. of the American Society of Civil Engineers, Vol. 103(HY12):1375-1389, 1977.

Cunningham, R. Segmenting binary images. Robotics Age, Vol 3(4):4-19, 1981.

Currie, I. G. Fundamental Mechanics of Fluids. McGraw-Hill Book Company, New York, 1974.

Davies, T. R. H. and A. J. Sutherland. Extremal hypotheses for river behavior. Water Resources Research, Vol. 19(1):141-148, 1983.

DeVantier, B. A. and B. E. Larock. Sediment transport in stratified turbulent flow. Journal of Hydraulic Engineering, Vol. 109(12):1622-1635, 1983.

Dickey, E.A., D.P. Jasa and T.R. Peterson. Tillage, residue and erosion on moderately sloping soils. TRANS of ASAE, pp. 1093-1099, 1984.

Dooge, J. C. I., W. G. Strupczewski and J. J. Napiorkowski. Hydrodynamic derivation of storage parameters of the Muskingum model. Journal of Hydrology, Vol. 54:371-387, 1982.

Drew, D. A. Mathematical modeling of two-phase flow. Ann. Rev. Fluid Mech., Vol. 15:261-291, 1983.

Einstein, H. A. The bed-load function for sediment transportation in open channel flows. Technical Bulletin No. 1026, USDA-SCS, Washington, D.C., 1950.

Foster, G. R. Modeling the erosion process. In Hydrologic Modeling of Small Watersheds, Ed. Haan et al., ASAE Monograph No. 5, St. Joseph, MI., 1982.

Graf, W. H. Hydraulics of Sediment Transport. McGraw-Hill Book Company, New York., 1971.

Gray, W. G. A derivation of the equations for multi-phase transport. Chemical Engineering Science, Vol. 30:229-233, 1975.

Greenberg, M. D. Foundations of Applied Mathematics, Prentice-Hall Inc., Englewood Cliffs, NJ., 1978.

Griffiths, G. A. Extremal hypotheses for river regime: An allusion of progress. Water Resources Research, Vol. 20(1): 113-118, 1984.

Hinze, J. O. Turbulence. Second Edition, McGraw-Hill Book Company, New York, 1975.

Keulegan, G. H. Laws of turbulent flow in open channels. Research Paper RP1151. Part of J. of Research of the National Bureau of Standards, Vol. 21, 1938.

Langbein, W. B. and L. B. Leopold. River meanders - theory of minimum variance. Geological Survey Professional Paper 422-H, 1966.

Leopold, L. B. and W. B. Langbein. The concept of entropy in landscape evolution. Geological Survey Professional Paper 500-A, 1962.

Leopold, L. B., M. G. Wolman and J. P. Miller. Fluvial Processes in Geomorphology. W. H. Freeman and Company, San Francisco, California, 1964.

Line D. E. and L. D. Meyer. 1987. Flow velocities of concentrated runoff along cropland furrows. ASAE Paper No. 87-2087, ASAE, St. Joseph, MI 49085.

Prigogine, I. Thermodynamics of Irreversible Processes. John Wiley & Sons, New York, 1967.

Rice, C., B. N. Wilson and M. Appleman. Instrumentation for erosion research using image processing techniques. ASAE Paper No. 87-2097, ASAE St. Joseph, MI 49085,1987a.

Rice, C., B. N. Wilson, M. Appleman and J.W. Brown. Measuring dynamic changes in rill flows. ASAE Paper No. 87-2577, ASAE St. Joseph, MI 49085,1987b.

Rice, C., B. N. Wilson and M. Appleman. Soil topography measurements using image processing techniques. In Press, Computers and Electronics in Agriculture, 1988a.

Rice, C., B. N. Wilson, M. Appleman and J.W. Brown. Image processing system for measuring surface velocities. In press, Applied Engineering in Agriculture, 1988b.

Rohlf, R. A. and M. E. Meadows. Dynamic mathematical modeling of rill erosion. ASCE Proc. Symp. on Watershed Management, Boise, ID,1980.

Rouse, H. Modern conceptions of the mechanics of fluid turbulence (closure). Trans. ASCE, Paper #1965, 1938.

Ruffini, J. and B. N. Wilson. Evaluation of Muskingum's parameters for ungaged watersheds. ASAE Paper No. 85-2018, ASAE St. Joseph, MI. 49085, 1985.

Schlichting, H. Boundary-Layer Theory. Seventh Edition, McGraw-Hill Book Company, New York, 1979.

Simons, D. B. and F. S. Senturk. Sediment Transport Technology. Water Resources Publications, Ft. Collins, Colorado, 1976.

Song, C. C. S. and C. T. Yang. Velocity profiles and minimum stream power. Journal of the Hydraulics Division, Proc. of the American Society of Civil Engineers, Vol. 105(HY8):981-998, 1979.

Song, C. C. S. and C. T. Yang. Minimum stream power: theory. Journal of the Hydraulics Division, Proc. of the American Society of Civil Engineers, Vol. 106(HY9):1477-1487, 1980.

Song, C. C. S. and C. T. Yang. Minimum energy and energy dissipation rate. Journal of the Hydraulics Division, Proc. of the American Society of Civil Engineers, Vol. 108(HY5):690-706, 1982.

Standart, G. The mass, momentum and energy equations for heterogeneous flow systems. Chemical Engineering Science, Vol. 9:227-236, 1964.

Vanoni, V. A. Transportation of suspended sediment by water. Transactions of the ASCE, Vol. 111:67-133, 1946.

Vanoni, V. A. and G. N. Nomicos. Resistance properties of sediment-laden streams. Transactions of the ASCE, Vol. 125: 1140-1175, 1960.

Wark, K. Thermodynamics. Second Edition, McGraw-Hill Book Company, New York, 1971.

Whitaker, S. Advances in theory of fluid motion in porous media. Industrial and Engineering Chemistry, Vol. 61(12):14-28, 1969.

Whitaker, S. The transport equations for multi-phase systems. Chemical Engineering Science, Vol. 28:139-147, 1973.

White, W. R., R. Bettes and E. Paris. Analytical approach to river regime. J. of the Hydraulics Div., Proc. of the ASCE, Vol. 108(HY10):1179-1193,1982.

Wilson, B. N. and B. J. Barfield. A detachment model for non-cohesive sediment. Transactions of ASAE, In press, 1986a.

Wilson, B. N. and B. J. Barfield. Predicted and observed turbulence in detention ponds. Accepted for publication in the Trans. of ASAE, 1986b.

Wilson, B. N. and C. Rice. Large-scale laboratory apparatus for erosion studies. ASAE Paper No. 87-2096, Presented at the ASAE Summer Meeting, St. Joseph, MI, 1987.

Yang, C. T. Potential energy and stream morphology. Water Resources Research, Vol. 7(2):311-322, 1971a.

Yang, C. T. Formation of riffles and pools. Water Resources Research, Vol. 7(6):1567-1574, 1971b.

Yang, C. T. Unit stream power and sediment transport. J. of the Hydraulics Div., Proc. of the ASCE, Vol. 98(HY10):1805-1826, 1972.

Yang, C. T. Minimum unit stream power and fluvial hydraulics. J. of the Hydraulics Div., Proc. of the ASCE, Vol. 102(HY7):919-934, 1976.

Yang, C. T. Minimum unit stream power and fluvial hydraulics (Closure). J. of Hydraulics, ASCE, Vol. 104(HY1):122-125, 1978.

Yang, C. T. Minimum rate of energy dissipation and river morphology. Proc. of the D. B. Simons Symp. on Erosion and Sedimentation, Ft. Collins, Colorado, 1983.

Yang, C. T. and C. C. S. Song. Theory of minimum rate of energy dissipation. J. of the Hydraulics Div., Proc. of the ASCE, Vol. 105(HY7):769-784, 1979.

Yang, C. T, C. C. S. Song and M. J. Woldenberg. Hydraulic geometry and minimum rate of energy dissipation. Water Resources Research, Vol. 17(4):1014-1018, 1981.